Superconducting micronets: A state-variable approach

Herman J. Fink and Stephen B. Haley
Department of Electrical Engineering and Computer Science, University of California, Davis, Davis, California 95616
(Received 18 June 1990; revised manuscript received 26 November 1990)

A state-variable formulation of the nonlinear Ginzburg-Landau equations for superconducting micronets is introduced. The state variables are the Cooper-pair density N, kinetic energy E, and the imaginary part I of the Cooper-pair momentum density $\mathcal{P}$. Purely algebraic relations among the state variables are derived, and several fundamental properties of micronets are proven. The current density $J=\mathrm{Re}\mathcal{P}$ is given by $J^2=NE-I^2$, where $I=\mathrm{Im}\mathcal{P}$. For the limit $N\ll 1$, a quasilinear theory yields the superfluid velocity Q as the only relevant transport parameter at the phase-transition boundary. Applying the full nonlinear theory, the maximum supercurrent that can be injected into a microladder is calculated as a function of normalized nodal spacing $\mathcal{L}/\xi(T)$ and magnetic flux ϕ for low magnetic fields, where $\xi(T)$ is the temperature-dependent coherence length. The critical current J_c approaches zero at a new temperature-critical flux boundary, $\phi_{c1}(T)$, which is first order and distinct from the second-order phase-transition boundary, $\phi_{c2}(T)$.

I. INTRODUCTION

Superconducting circuits for which the distance between nodes is of the order of magnitude of the coherence length $\xi(T)$ are called microcircuits (MC). Future implementation of superconducting micronets in microcircuitry will require not only characterization of superconducting devices in a network, but also a fundamental understanding of the critical currents of the network and of the phase-transition boundaries. In a magnetic field, MC's undergo a second-order phase transition (SOPT) at the superconducting-normal state boundary. Starting with the work of de Gennes,[1] phase-transition boundaries have been calculated for many circuit topologies.[2–8] Such calculations are relatively straightforward since only the linearized Ginzburg-Landau (GL) equations are required. When currents from an external source are injected into a MC, the nonlinear GL equations have to be used since, at the critical current (maximum loss-free time-independent current), the phase transition is no longer of second order. Even in the case when only persistent currents, generated by a magnetic flux linking the circuit, are present, the nonlinear GL equations have to be used.

We introduce a real-state-variable formulation of the one-dimensional, complex nonlinear GL equation, applicable to micronets. The state variables—Cooper-pair density N, kinetic energy E, and imaginary part I of the Cooper-pair momentum density $\mathcal{P}$—are coupled by first-order nonlinear differential equations which can be integrated to yield algebraic relations among N, E, and I, where $I=\mathrm{Im}\mathcal{P}$. The current density J is algebraically linked to the state variables by $J^2+I^2=NE$. This state-variable formulation, although entirely equivalent to the usual complex-order-parameter approach, yields additional physical insight, and it forms a convenient basis for both analytical and numerical analysis of MC's. For any MC we prove that N and E assume opposite extremum values at points where the order parameter ψ is a momentum eigenfunction, and that the difference between the kinetic and condensation energies is always constant along any network branch.

From a quasilinear theory, valid near a second-order phase-transition boundary, an exact solution is developed for the superfluid velocity Q. At this boundary, Q is the only relevant nonzero transport parameter.

As an application, we consider the superconducting microladder circuit whose SOPT boundary was explored[3] shortly after the introduction of microcircuit concepts.[1–4] The ladder is a particularly good example since it bears a similarity to a thin solid film in a magnetic field parallel to its surface. The ladder is also important for an understanding of flux shuttling, and it is the basic topology for conventional filter circuits. Near the SOPT boundary, the ladder allows a vortex state[3] in certain flux regions, like a thin film.[9] It was shown in Ref. 3 for $\phi<0.215\phi_0$ (ϕ_0 is the fluxoid quantum $hc/2|e|$) that the ladder may permit a current state near the SOPT boundary which is similar to the shielding current of a thin film or that of a bulk superconductor in the Meissner state.

In this work, we calculate the critical current J_c when a transport current is superimposed on a shielding current. An additional first-order critical-current–magnetic-flux phase boundary is found, and explained on the basis of a free-energy analysis. In other MC studies, exact solutions of critical transport currents have been calculated for an infinite superconducting square network in *zero* magnetic field,[10] for a superconducting wire with very long side branches,[11] and for a superconducting quantum interference device (SQUID).[12] An alternative approach using the linearized GL equation was explored by the authors of Refs. 13 and 14. As will become apparent, such an approach is inapplicable.

II. BASIC THEORY: REAL-STATE VARIABLES

A. Nonlinear theory

In this section a formulation with use of the one-dimensional GL equations is developed, which is applic-

able to micronetworks composed of wires of uniform cross section. Usually, the GL equations are formulated as a nonlinear second-order differential equation for the complex order parameter ψ and an expression for the supercurrent density J in terms of $|\psi|$, the gradient of the phase of ψ, and the magnetic vector potential $\mathbf{A}$. In lieu of this approach, we introduce a set of three real variables N, E, and I, in addition to J, which satisfy a set of coupled first-order state-variable equations.

The one-dimensional GL equation for the complex order parameter ψ, normalized by its value $\psi(\infty)$ at zero field and current at fixed temperature, is

$$(\hat{p}^2-1+|\psi|^2)\psi(x)=0 . \tag{2.1}$$

The coordinate x on a branch is normalized by the temperature-dependent coherence length

$$\xi(T)=\xi(0)[1-(T/T_c)^2]^{1/2} .$$

The operator $\hat{p}$ is the projection of a normalized momentum operator onto x. It is defined in terms of the conventional momentum operator p by

$$\hat{p}=\frac{\xi}{\hbar}p=-i\frac{\partial}{\partial x}+\mathcal{A}(x) ,$$

where $\mathcal{A}=2\pi\xi A/\phi_0$, with A being the component of the magnetic vector potential along x and with ϕ_0 being the fluxoid quantum $hc/2|e|$.

The four real variables are defined as follows:

$$N(x)=|\psi|^2 , \tag{2.2a}$$

$$E(x)=|\hat{p}\psi|^2 , \tag{2.2b}$$

$$I(x)=\mathrm{Im}\mathcal{P}(x) , \tag{2.2c}$$

$$J(x)=\mathrm{Re}\mathcal{P}(x) , \tag{2.2d}$$

where $\mathcal{P}(x)$ is the Cooper-pair momentum density,

$$\mathcal{P}(x)=\psi^*\hat{p}\psi .$$

The physical meaning of N, E, I, and J will become more apparent when ψ is expressed in the modulus-phase form,

$$\psi(x)=f(x)e^{i\theta(x)} ,$$

so that expressions (2.2) are written as

$$N=f^2 , \tag{2.3a}$$

$$E=\left[\frac{df}{dx}\right]^2+f^2\left[\mathcal{A}+\frac{d\theta}{dx}\right]^2 , \tag{2.3b}$$

$$I=-f\frac{df}{dx} , \tag{2.3c}$$

$$J=f^2\left[\mathcal{A}+\frac{d\theta}{dx}\right] . \tag{2.3d}$$

It is clear that N is the normalized Cooper-pair density and the variable E is the Cooper-pair kinetic-energy density. The normalized current density J is related to the conventional quantum-mechanical current density by

$$J_{\mathrm{conv}}=(|e|\hbar|\psi(\infty)|^2/2m\xi)J$$
$$=(Jc\phi_0)/(8\pi^2\xi\lambda^2) ,$$

where λ is the GL penetration depth. The current J is proportional to the gradient of the phase of ψ and the vector potential. The state variable I arises from the gradient of the pair density N. If I is written in conventional units, it has units of current density, but is should not be likened to a diffusion current, such as those found in semiconductors. Although $I(x)$ is, in general, nonzero at any given point in a MC, there always exist (at least at zero frequency) compensating gradients such that I carries no net transport or circulating current. This point will be further clarified in the discussion on the microladder in Sec. III. Another point worthy of mention is that the state variables are gauge invariant.

Differentiating the variables in (2.2) and using (2.1) to eliminate second derivatives leads to a set of nonlinear coupled state-variable equations. It is

$$\frac{dN}{dx}=-2I , \tag{2.4a}$$

$$\frac{dE}{dx}=2(1-N)I , \tag{2.4b}$$

$$\frac{dI}{dx}=(1-N)N-E , \tag{2.4c}$$

$$\frac{dJ}{dx}=0 . \tag{2.4d}$$

From (2.4d) one sees that J is constant along a branch, as expected, since we assume one-dimensional transport. Note that J is not coupled to the state variables in (2.4); however, it follows directly from the definitions in (2.2) that all of the state variables are linked by the constraint

$$\mathcal{P}^*\mathcal{P}=J^2+I^2=NE . \tag{2.5}$$

Values of J and N in the branches, forming a loop, are related to the magnetic flux locked in the loop by integrating the expression for J in (2.3) around the loop. This gives the fluxoid quantum condition

$$\Gamma\equiv 2\pi\left[n+\frac{\phi}{\phi_0}\right]=\oint\frac{J}{N(x)}dx , \tag{2.6}$$

with n an integer or zero.

A fundamental result follows immediately from the definition

$$I(x)=\mathrm{Im}[\psi^*(x)\hat{p}\psi(x)]$$

and the state-variable equations. If the order parameter $\psi(x)$ is an eigenstate of the momentum operator $\hat{p}$ in the neighborhood of a point $x=x_0$, then $I(x_0)=0$. At such a point, the pair density $N(x_0)$ and the pair kinetic-energy density $E(x_0)$ assume opposite extremum values, as seen from (2.4a) and (2.4b). Conversely, ψ is not an eigenfunction of $\hat{p}$ where N and E are not extrema. As we shall show, the presence of extrema plays an important role in simplifying the analysis of MC's.

To solve (2.4) on a micronet, nodal boundary conditions are introduced. Consider an arbitrary node m con-

nected to another node n by branch α. Let x_α be measured from an arbitrary point on branch α to node m. The single valuedness of ψ at node m requires the nodal condition

$$N(x_\alpha)=N(x_\beta)=\cdots \ . \tag{2.7}$$

A second fundamental condition is the conservation of complex momentum density at node m:

$$\sum_\alpha \mathcal{P}(x_\alpha)=0 \ .$$

This is equivalent to the real, conservation conditions

$$\sum_\alpha J_\alpha=0$$

and (2.8)

$$\sum_\alpha I(x_\alpha)=0 \ ,$$

where the summation is taken outward from node m over all branches connected to node m. It follows from (2.4a) that conservation of I is equivalent to requiring the sum of the derivatives of N at node m to be zero.

The state-variable equations (2.4), the constraint (2.5), and the fluxoid condition (2.6), together with the nodal conditions (2.7) and (2.8), contain all information about superconducting micronets consistent with the GL equations. In order to resolve (2.4) the individual equations will be decoupled. Combining (2.4a) and (2.4b) and integrating, it follows that N and E have the important relation

$$E(x)-F(x)=E(x_0)-F(x_0)=C \ , \tag{2.9}$$

where

$$F(x)=-N(x)[1-\tfrac{1}{2}N(x)]<0$$

is the normalized pair condensation energy density, and C is a constant, i.e., x_0 is arbitrary. Equation (2.9) explicitly shows that any change in the kinetic-energy density, due to variation of parameters such as persistent and injected currents, is exactly compensated by a change in condensation energy density at every point x.

The GL equation (2.1) is a consequence of minimizing the Gibb's free energy with respect to variation in the order parameter ψ. In terms of our state variables, the Gibb's free-energy density, after minimization, is $G(x)=E(x)+F(x)$. The magnetic-energy density due to the self-field term of the vector potential arising from the current density in the filaments is negligible for idealized MC's with a vanishing wire cross section. Using (2.4c) and the definition of $F(x)$ yields

$$G(x)=-\tfrac{1}{2}N^2(x)-\frac{dI(x)}{dx}$$
$$=-\tfrac{1}{2}\left[N^2(x)-\frac{d^2N(x)}{dx^2}\right] \ .$$

Although the integral of $G(x)$ along a network branch depends on I at the ends of the branch, the total Gibb's free energy for a MC is independent of I, which follows directly from the nodal condition (2.8). Thus, the total Gibb's free energy of an ideal MC is given by

$$G=-\tfrac{1}{2}\sum_\alpha \int dx_\alpha N^2(x_\alpha) \ , \tag{2.10}$$

where the sum is over all branches of the network. As will be shown in Sec. IV, (2.10) is the key to understanding the physical basis for the critical-current phase-transition boundary.

Eliminating E from (2.5) and using (2.9) leads to the equation

$$I^2(x)=\frac{1}{4}\left[\frac{dR}{dx}\right]^2=R(b^2+a^2R+\tfrac{1}{2}R^2)+I_0^2 \ , \tag{2.11}$$

where $R(x)=N(x)-N_0$ and

$$a^2=\tfrac{3}{2}N_0-1 \ ,$$
$$b^2=E_0-(1-N_0)N_0=0.5(d^2N/d^2x)|_{x_0} \ . \tag{2.12}$$

The values of the state variables at the arbitrary point x_0 are N_0, E_0, and I_0. As an algebraic equation relating state variables, (2.11) shows that $I^2(x)$ is a cubic function of $N(x)$. On the other hand, (2.11) is an inhomogeneous nonlinear differential equation for $R(x)=N(x)-N_0$, which many be written in terms of an elliptic integral. In general, an analytic solution does not exist. However, the following extremum-referencing procedure can be used to simplify (2.11).

Let x_0 be a point where $dN/dx=0$. In this case $I_0=0$, and (2.11) reduces to a homogeneous equation in $R(x)$ whose solution is the square of Jacobian elliptic, spatially periodic functions of x with parameters N_0 and E_0. However, without solving (2.11), one can learn a great deal about the behavior of the solutions by considering the relation $J^2=N_0E_0$ and b^2. There are four distinct solutions of (2.11) which correspond to the following branch current conditions: If $J\neq 0$ then both N_0 and E_0 are nonzero, and either $b^2<0$ for N_0 a maximum or $b^2>0$ for N_0 a minimum. The case $b^2=0$ gives $J^2=(1-N_0)N_0^2$, which is the expression for the current in a long wire or ring. If $J=0$ then either N_0 or $E_0=0$. If $E_0=0$, then N_0 is a maximum and $b^2<0$. If $N_0=0$, then E_0 is a maximum and $b^2>0$. For $J=0$, the pair density $N(x)$ is periodic and both extrema of $N(x)$ and $E(x)$ exist. The case $N_0=E_0=0$ with $J=0$ exists only if there is an extended normal region, $N(x)=0$, otherwise (2.11) is not satisfied.

Equation (2.11) is a convenient form to develop approximate nonlinear analytic solutions. The basic assumption is that the pair density $N(x)$ on a branch does not deviate much from its extremum value N_0. This assumption is implemented by neglecting the term R^3 in (2.11) with $I_0=0$. The resulting equation has the solution

$$N(x)=N_0+\left[\frac{b}{a}\right]^2\sinh^2(ax) \ , \tag{2.13}$$

where x is measured from the extremum of $N(x)$. This approximate solution of (2.11) is valid where $R\ll 2|a^2|$. In the same approximation, (2.11) can also be integrated

analytically with I_0 present. To obtain an estimate of the accuracy of (2.13), consider the power-series solution of (2.11),

$$N(x)=N_0+b^2x^2\left[1+\frac{a^2}{3}x^2+\frac{1}{5}\left[\frac{2}{9}a^4+\frac{b^2}{2}\right]x^4+\cdots\right] . \tag{2.14}$$

Comparing an expansion of (2.13) in terms of ax with (2.14) shows that the first error term is $b^4x^6/10$. Hence, (2.13) is expected to be quite accurate for small $b^{2/3}x$.

B. Quasilinear theory

Near the second-order phase boundary, the value of $N\equiv|\psi|^2\ll 1$. Linearizing the GL equation (2.1) by neglecting $|\psi|^3$ is equivalent to linearizing the state-variable equations (2.4) by neglecting N compared to unity. However, J remains linked to the other state variables by the exact nonlinear constraint (2.5). The resulting "quasilinear theory" leads to the equation

$$(dR/dx)^2=4R(E_0-N_0-R) . \tag{2.15}$$

The solution of (2.15) is

$$N(x)=N_0+(E_0-N_0)\sin^2x =N_0[1+(Q_0^2-1)\sin^2x] , \tag{2.16}$$

where $Q_0=\pm\sqrt{E_0/N_0}=J/N_0$ is the superfluid velocity at the point $x=0$ where $N(x)$ is an extremum. Equation (2.16) may also be obtained from the hyperbolic solution (2.13) by setting $a^2=-1$ and $b^2=E_0-N_0$. Since $Q_0^2=1+b^2/N_0$, it follows that $Q_0^2>1$ for N_0 a minimum and $Q_0^2<1$ for N_0 a maximum.

Near a second-order phase-transition boundary, N, E, and J approach zero. In contrast, the superfluid velocity $Q(x)=J/N(x)$ does not, in general, approach zero, and is thus the only relevant transport parameter at a second-order phase-transition boundary. It follows from (2.16) that

$$Q(x)=Q_0[1+(Q_0^2-1)\sin^2x]^{-1} \quad \text{for } J\neq 0 . \tag{2.17}$$

It is evident, if $Q_0=1$ then $Q(x)=1$ for all x. This case occurs for long wires, isolated loops, and certain highly symmetric infinite lattices.[15] If $J=0$ and $N_0\neq 0$ then $E_0=0$ and $Q(x)=0$ for all x, and if $N_0=0$ then E_0 is finite and $Q(x)$ is a Dirac δ function. This singular case is important in certain periodic two-dimensional networks.[15]

Substituting (2.16) into the nodal conditions (2.7) and (2.8), using $2I=-dN/dx$ and

$$J=N(x)Q(x)=N_0Q_0 ,$$

leads to

$$N_{0\alpha}[1+(Q_{0\alpha}^2-1)\sin^2x_{m\alpha}] =N_{0\beta}[1+(Q_{0\beta}^2-1)\sin^2x_{m\beta}]=\cdots ,$$

$$\sum_\alpha N_{0\alpha}Q_{0\alpha}=0 ,$$

and (2.18)

$$\sum_\alpha N_{0\alpha}(Q_{0\alpha}^2-1)\sin 2x_{m\alpha}=0$$

for node m, where $Q_{0\alpha}=J/N_{0\alpha}$ is the superfluid velocity on branch α at the extremum point $x_\alpha=0$.

Using (2.17), the fluxoid quantization condition (2.6) leads to

$$\Gamma=\sum_\alpha[\arctan(Q_{0\alpha}\tan x_{m\alpha})+\arctan(Q_{0\alpha}\tan x_{n\alpha})] . \tag{2.19}$$

In Eqs. (2.18) and (2.19), $x_{m\alpha}$ and $x_{n\alpha}$ are positive. In (2.19) the sum is over all branches forming a loop enclosing ϕ/ϕ_0. It is evident that, for at least one branch, the superfluid velocity $Q_{0\alpha}$ must be nonzero at the phase boundary when the magnetic flux is nonzero. Equation (2.19) is analogous to Kirchhoff's voltage law, except that here phase differences are summed.

The quasilinear theory contains more information than the linear complex-order-parameter ψ equation of de Gennes[1] and Alexander.[4] Since the homogeneous equations (2.18) are linear in $N_{0\alpha}$, only ratios $N_{0\alpha}/N_{0\beta}$ can be determined. In contrast, the nonlinear dependence on $Q_{0\alpha}$ permits an explicit solution for $Q_{0\alpha}$, and hence for $Q(x)$ using (2.17), as demonstrated in Sec. IV.

III. SQUARE LADDER: EXACT SOLUTIONS

With use of the linearized Ginzburg-Landau theory, the second-order phase-transition boundary between the superconducting and normal states of the infinite square microladder [Fig. 1(a)] has been calculated.[3] Figure 1(b) shows the second-order phase-transition boundary in terms of the normalized nodal spacing $\mathcal{L}/\xi(T)$ as a function of normalized magnetic flux ϕ/ϕ_0. Increasing values on the $\mathcal{L}/\xi$ axis correspond to decreasing temperature if $\mathcal{L}$ and $\xi(0)$ are fixed. The zero-flux, zero-current transition temperature T_c corresponds to $\mathcal{L}/\xi=0$. The transition temperature is a periodic function of magnetic flux. Only the first cycle is shown in Fig. 1(b). Also shown is the normalized wave vector q of ψ at the second-order phase-transition boundary. The inverse of the latter is a measure of the spatial period of a likely current-vortex pattern in the superconducting state very close to the second-order phase-transition boundary. For $\phi<0.215\phi_0$, the value of $q=0$, implying an infinite period, corresponds to a very long current loop, comparable to the shielding current in a thin-film or bulk superconductor below H_c or H_{c1}. We anticipate that this uniform current mode exists in the superconducting state, away from the phase-transition boundary but not necessarily over the same magnetic flux interval. Currents in all transverse branches in Fig. 1(a) are zero for the uniform current mode, by definition. Here we consider critical currents "deep" in the superconducting domain, i.e.,

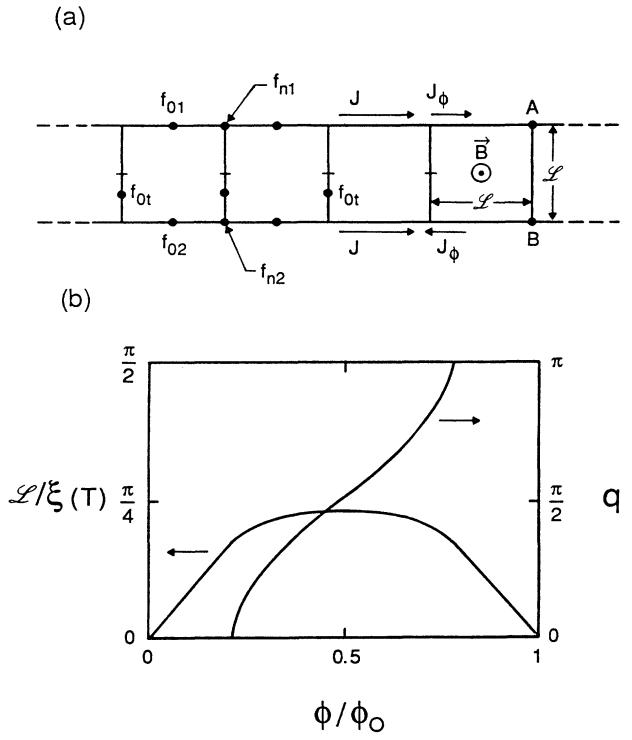

FIG. 1. (a) Shown is a section of an infinite ladder, where J is the external injected current and J_ϕ that due to magnetic shielding. f_{01}, f_{0t}, and f_{02} are extrema of $|\psi|$, with their locations indicated. (b) The second-order phase-transition boundary of the infinite ladder: $\mathscr{L}/\xi(T)$ vs ϕ/ϕ_0 of Ref. 3.

$\mathscr{L}/\xi(T)$ is much larger than its value at the phase-transition boundary, shown in Fig. 1(b). Thus, the complete nonlinear GL equations must be used.

For computational and conceptual expediency, we analyze the microladder by investigating the critical current of a thin wire with side arms of length $a=\alpha\mathscr{L}/2$, shown in Fig. 2(a). The length $\mathscr{L}$ is the distance between the nodes, and α is a parameter for adjusting the appropriate length of the arms so that two such wires can be linked together to form a microladder.

When the magnetic flux in each unit cell is zero, we expect that the persistent current J_ϕ, shown in Fig. 1(a), is zero and the current in the upper branch $J_1=J+J_\phi$ is equal in magnitude and direction to the current in the lower branch $J_2=J-J_\phi$. Because of symmetry, the position of the extremum of the transverse order parameter (OP) (modulus of ψ) f_{0t}, is located at the center of the transverse branch, and $f_{01}=f_{02}$, $f_{n1}=f_{n2}$, $J_1=J_2$, and $a=\mathscr{L}/2$.

When the magnetic flux $\phi\neq 0$, then $J_\phi\neq 0$ and $J_1>J_2$ (the applied magnetic flux density **B** is pointing out of the paper in accordance with Lenz's law). In that case, the position of the maximum of the OP in the transverse branch moves away from the center. When f_{0t} is located on the transverse branch between nodes A and B [see Fig. 1(a)], the spatial variation of the OP on the ladder can be constructed by use of a wire with side arms of

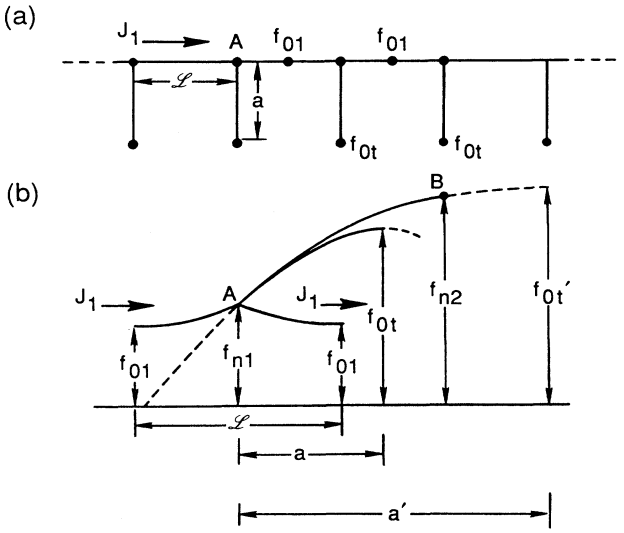

FIG. 2. (a) Infinite wire with side arms with current $J_1=J+J_\phi$. This is a building block for constructing OP solutions of the ladder. (b) Schematic of spatial variation of the OP along the longitudinal and transverse branches of the ladder shown above.

length $a=\alpha\mathscr{L}/2$ [see Fig. 2(a)], and another wire with side arms of length $(2-\alpha)\mathscr{L}/2$. Since, at the ends of the arms, the slope of the OP is zero, the two wires can be matched provided the values of the OP's at the ends of the arms are the same.

Figure 2(b) schematically shows the expected behavior of the OP's of the branches connected to node A, as confirmed by numerical computation. The OP of the branch which carries the current J_1 has a minimum f_{01}, while the transverse branch, without a current, has a maximum f_{0t}. This follows from the nodal condition that requires the sum of the slopes of the OP's, taken radially outward from a node, to be zero. Furthermore, values of the moduli of the OP's of the various branches meeting at A must be the same.

If f_{0t} is located between f_{n1} and f_{n2}, then f_{02} is a minimum, which follows from the nodal condition since the slope of the transverse branch at f_{n2} is upward. When $\alpha=2$, then f_{0t} is located at node B. Then all slopes at node B are zero, and the OP in branch 2 is spatially constant so that $f_{0t}=f_{n2}=f_{02}$. A further change of the current in branches 1 and 2 may shift the maximum of the transverse *function* outside the ladder. This requires an extrapolation of the OP function of the transverse branch $f_t(x)$ beyond f_{n2}, to a maximum f'_{0t}, a distance a' from A, shown in Fig. 2(b). In this case, f_{02} corresponds to the maximum OP in branch 2, even though J_2 is nonzero.

The spatial variations of the OP's for $\alpha<2$ and $\alpha>2$, resulting from numerical calculations, are depicted schematically in three dimensions in Figs. 3(a) and 3(b). When $\alpha<2$, a solution at node B is constructed in the same way as is done at node A, except that α is replaced by $\alpha'=(2-\alpha)$. When $\alpha>2$, one may construct a solution at node B by considering a wire with arms of length

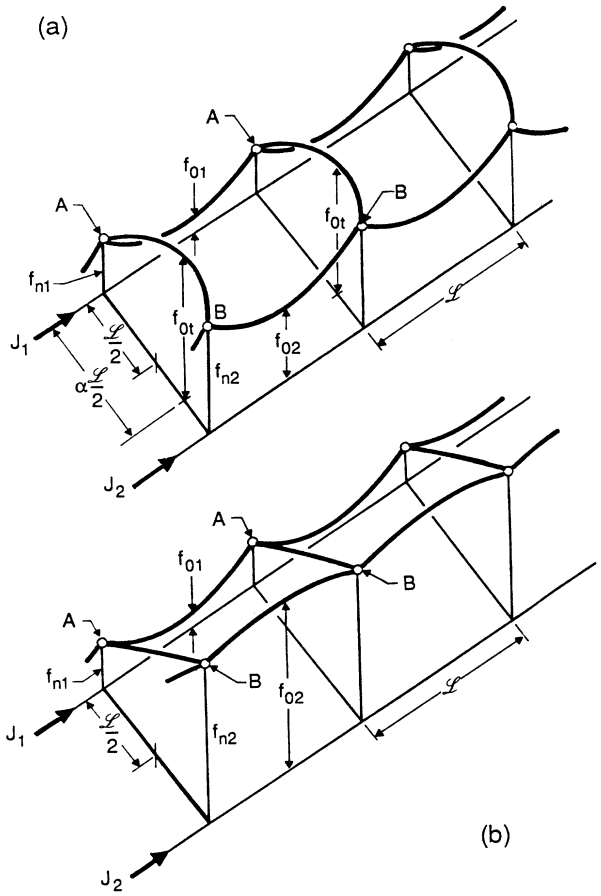

FIG. 3. Three-dimensional schematic of spatial variation of the OP when (a) the maximum of the transverse branch order parameter f_{0t} is between nodes A and B, and (b) when it is outside A and B, on an extrapolation of the transverse branch function (not shown in this figure) as indicated by f'_{0t} in Fig. 2(b). Note that, for (a), the OP in branch 2 has minima, and for (b) it has maxima.

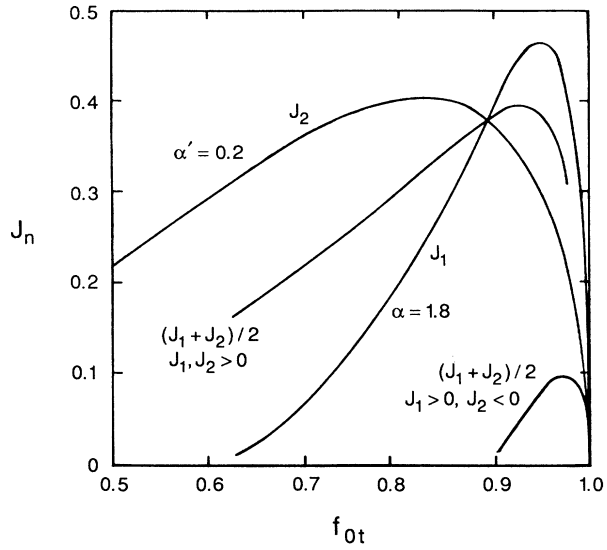

FIG. 4. Functional dependence of currents J_1 and J_2 in wires with arms of length $1.8\mathcal{L}/2$ and $0.2\mathcal{L}/2$ on the OP at the end of the arms, f_{0t}, for $\mathcal{L}/\xi=\pi/2$. [See Fig. 2(a).] This corresponds to a ladder solution when f_{0t} is the same for both wires with currents: $J_1=J+J_\phi$ and $J_2=J-J_\phi$. The maximum of $(J_1+J_2)/2$ is the critical current for the above parameters. There are two solutions: J_1 and J_2 parallel or antiparallel.

$\beta\mathcal{L}/2$, where $\beta=\alpha-2$, with the length $\beta\mathcal{L}/2$ corresponding to the extrapolated part of $f_t(x)$. All slopes of this solution are positive at node B. Alternatively, one can take the minimum of $f_t^2(x)$ as a reference point instead of the maximum. Then the slopes of $f(x)$ at node B on branch 2 and on the transverse branch are of opposite sign.

In solving the critical-current problem, the one-dimensional GL equation (2.11) with $I_0=0$ was used. This assumes that the wire diameter of the ladder is smaller than or equal to $\lambda(T)$ and $\xi(T)$. Equation (2.11) depends on two parameters: $N_0\equiv f_0^2$ and $J^2=N_0E_0$. Solutions of (2.11) were matched at the nodes, using the nodal conditions (2.7) and (2.8).

The numerical procedure was centered around a search of f_{01} and f_{0t} [see, e.g., Fig. 2(a)], for fixed $\mathcal{L}/\xi$, a/ξ, and J. After finding a solution, a different value of J was used in the search for the next solution, keeping $\mathcal{L}/\xi$ and a/ξ fixed. The results shown in Figs. 4–7 were calculated with $\mathcal{L}/\xi(T)=\pi/2$, which is far away from the second-order phase-transition boundary, shown in Fig. 1(b). Figure 4 shows the current in branch 1, J_1, for arm length $a_1=1.8\mathcal{L}/2$, and the current in branch 2, J_2, for arm length $a_2=0.2\mathcal{L}/2$ as a function of f_{0t}. For each value of f_{0t} the two corresponding currents J_1 and J_2 are solutions of the GL equations. The total injected current $2J=J_1+J_2$ has a maximum at some value $(f_{0t})_m$ that does not correspond to the maximum of either J_1 or J_2. This current is the maximum (or critical) supercurrent which can be injected into the ladder from an external

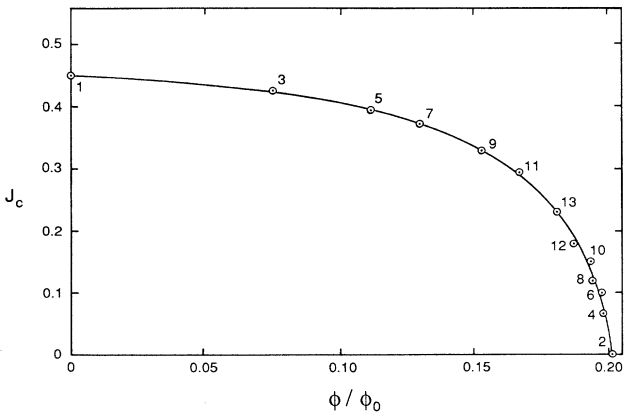

FIG. 5. Critical current as a function of magnetic flux (per unit cell $\mathcal{L}^2$) for the uniform current mode for $\mathcal{L}/\xi(T)=\pi/2$. The maxima of $(J_1+J_2)/2$ of Fig. 4 correspond to points 5 and 6. $J_c=0$ at $\phi/\phi_0\approx0.202$.

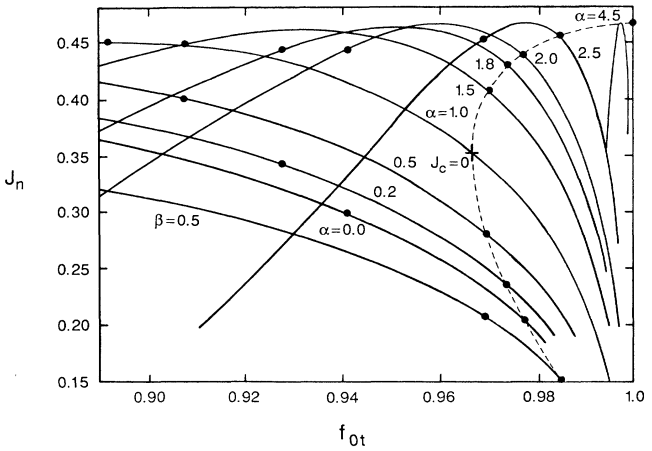

FIG. 6. Plots similar to those shown in Fig. 4 for various lengths of the side arms shown in Fig. 2(a). Dots to the right are solutions of the ladder critical current when $J_1>0$ and $J_2<0$, and to the left when $J_1>0$ and $J_2>0$. For details see text. $\mathcal{L}/\xi(T)=\pi/2$.

source, and the corresponding shielding current taken at the same $(f_{0t})_m$ is $J_\phi=(J_1-J_2)/2$. It should be noted that the signs of J_1 and J_2 can be the same or opposite, since (2.11) depends on J^2, giving rise to two solutions. The second solution, for $J_2<0$, is also shown in Fig. 4.

The flux per unit cell is calculated from the fluxoid quantization relation (2.6) with $n=0$:

$$\pi\frac{\phi}{\phi_0}=J_1\int_{x_{01}}^{x_{n1}}\frac{dx}{N_1(x)}-J_2\int_{x_{02}}^{x_{n2}}\frac{dx}{N_2(x)}\ . \tag{3.1}$$

Again, J_1 and J_2 can have the same or opposite signs. The first integral is extended from the minimum of $N_1(x)$ to node A and the second integral from the extremum of $N_2(x)$ to node B. For example, point 5 in Fig. 5 is the value of J_c shown in Fig. 4, with J_1 and J_2 parallel. The corresponding flux is calculated from (3.1) after the functions $N_1(x)$ and $N_2(x)$ had been calculated. When $J_\phi>J$, the current J_2 reverses direction and is flowing antiparallel to J_1. In this case, the critical current and $(f_{0t})_m$ are different from when J_1 and J_2 are parallel. That maximum J value, shown in Fig. 4 for $J_2<0$, leads to a larger value of flux and is point 6 in Fig. 5.

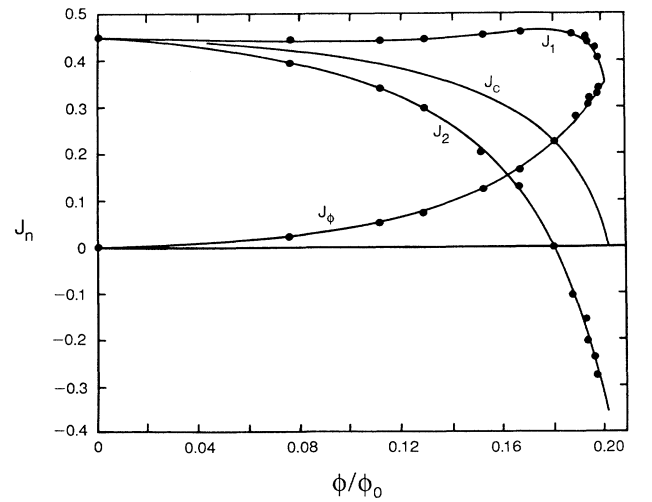

FIG. 7. Shown are the currents J_1 and J_2 in branches 1 and 2 of the ladder and $J_\phi=(J_1-J_2)/2$, corresponding to the critical current shown in Fig. 5. J_c is also shown here. $\mathcal{L}/\xi(T)=\pi/2$.

Figure 6 shows further data, similar to that in Fig. 4, for determining other values of J_c. For example, $\alpha=1.5$ and $\alpha'=0.5$ (points 3 and 4 in Fig. 5) or $\alpha=2.5$ and $\beta=0.5$ (points 9 and 10 in Fig. 5) are proper combinations. Also shown in Fig. 6 are values of J_1, J_2, and f_{0t} at which $|J_1|+|J_2|$ and $|J_1|-|J_2|$ are maxima. The solid circles converging to the left are for $|J_1|+|J_2|$, and those on the right for $|J_1|-|J_2|$. The solutions on the right converge to

$$J_1=-J_2=J_\phi=0.354\ ,$$

$f_{0t}=0.9665$ when $\alpha=\alpha'=1$, corresponding to $J_c=0$ and $\phi/\phi_0=0.202$. The other point on the $\alpha=1$ curve is located at its maximum. There $J_1=J_2=J_c=0.451$, corresponding to $f_{0t}=0.8920$, $J_\phi=0$, and $\phi=0$. The latter is the critical current when the magnetic flux per unit cell is zero.

Another point of special mention is $\alpha=2.0$ and $\alpha'=0$. The curve for $\alpha=0$ was calculated from $J=N_{0t}(1-N_{0t})^{1/2}$, that of a long wire without arms. In this case the extrema in branch 2 disappear and $f_2(x)$ is constant. Points 7 and 8 in Fig. 5 correspond to that particular case.

Figure 7 shows J_1, J_2, and J_ϕ, corresponding to J_c shown in Fig. 5, as a function of flux. The flux at which $J_c\to 0$ is 0.202. This does not mean that superconductivity disappears for flux larger than 0.202. As a matter of fact, all OP's are large there. For $\phi/\phi_0>0.202$, one expects a vortex state in the ladder with finite currents in the transverse branches.

The scatter in the calculated points of Figs. 5 and 7 for $0.18\lesssim\phi/\phi_0\lesssim 0.2$ arises from errors in the calculated flux, not the current. This is due to the graphical procedure used in the last step of the calculation as explained in connection with Fig. 4. The integrals of Eq. (3.1) are very sensitive to the correct functions $N_1(x)$ and $N_2(x)$, and these vary strongly near the maximum of J_1+J_2. The estimated error in ϕ/ϕ_0 is about ± 0.001.

IV. RECTANGULAR LADDER: ANALYTIC APPROXIMATIONS

In this section approximate analytic formulas for critical currents of a *rectangular* ladder are developed. The longitudinal branches, carrying currents J_1 and J_2, have normalized length $\mathcal{L}$, and the transverse branches which carry no current for the uniform mode, have normalized length $r\mathcal{L}$, where r is a scaling factor. The distance from an upper node [A in Fig. 1(a)] to the extremum point on a transverse branch is $\alpha\mathcal{L}/2$, as explained in Sec. III. Applying nodal conditions (2.7) and (2.8) with solution (2.13) to a node on branch 1 yields

$$N_{01}+\left[\frac{b_1}{a_1}\right]^2\sinh^2(a_1\mathcal{L}/2) =N_{0t}+\left[\frac{b_t}{a_t}\right]^2\sinh^2(a_t\alpha\mathcal{L}/2)\ , \quad (4.1)$$

and

$$2\frac{b_1^2}{a_1}\sinh(a_1\mathcal{L})=-\frac{b_t^2}{a_t}\sinh(a_t\alpha\mathcal{L})\ . \quad (4.2)$$

The quantities a and b, defined in (2.12), are functions of N_{01} and N_{0t}, the extrema of $N(x)$ on branch 1 and the transverse branch, respectively, and $E_{01}=J_1^2/N_{01}$. The nodal conditions for a branch 2 node are also given by (4.1) and (4.2) with the subscript 1 replaced by 2 and α replaced by $\alpha'=2r-\alpha$. For arbitrary values of $\mathcal{L}$, (4.1) and (4.2) cannot be solved analytically. The result of numerical computations based on (4.1) and (4.2) is discussed below. For now we develop series solutions accurate to order $\mathcal{L}^2$. The procedure used here treats the ladder intact, distinct from the numerical approach in Sec. III, where the ladder was linked together from single wires with dangling bonds.

Eliminating b_1 from (4.1) and (4.2), and expanding the result to order $\mathcal{L}^2$ [$O(\mathcal{L}^2)$] yields

$$N_{01}(\alpha)=N_{0t}-\tfrac{1}{8}(1-N_{0t})N_{0t}\alpha(1+2\alpha)\mathcal{L}^2\ . \quad (4.3)$$

Expanding (4.2) to $O(\mathcal{L}^3)$, noting that terms to $O(\mathcal{L})$ cancel, and using (4.3) leads to the current $J_1=\sqrt{N_{01}E_{01}}$:

$$J_1(\alpha)=\left[\frac{2+\alpha}{2}\right]^{1/2}\sqrt{1-N_{0t}}N_{0t}[1+(pN_{0t}-q)\mathcal{L}^2]\ , \quad (4.4)$$

where

$$p=\frac{1}{16}\frac{\alpha}{2+\alpha}(4\alpha^2+13\alpha+4)\ ,$$

$$q=\frac{1}{48}\frac{\alpha}{2+\alpha}(10\alpha^2+27\alpha+8)\ .$$

For convenience J_1 is always assumed positive. The current $J_2=\pm J_1(\alpha')$. The corresponding pair density is $N_{02}=N_{01}(\alpha')$. The injected current J per wire and the induced shielding current J_ϕ are

$$2J=J_1(\alpha)\pm J_1(\alpha')$$

and (4.5)

$$2J_\phi=J_1(\alpha)\mp J_1(\alpha')\ .$$

The upper sign denotes $J>J_\phi$ and the lower sign $J<J_\phi$. The currents J and J_ϕ are functions of the extremum N_{0t} and its position on the transverse branch. The parameters N_{0t} and α are related to the flux linking the ladder by the fluxoid quantization condition (2.6), which assumes, with $n=0$, the form

$$J_1\int_{-\mathcal{L}/2}^{\mathcal{L}/2}\frac{dx}{N_1(x)}-J_2\int_{-\mathcal{L}/2}^{\mathcal{L}/2}\frac{dx}{N_2(x)}=\chi\mathcal{L}\ , \quad (4.6)$$

where $\chi=(2\pi/\mathcal{L})\phi/\phi_0$, and $\mathcal{L}$ and x are normalized by $\xi(T)$.

Using (2.14), (4.6), and $J_2=\pm J_1(\alpha')$ leads to the following $O(\mathcal{L}^2)$ expression:

$$\chi=\left[\frac{1-N_{0t}}{2}\right]^{1/2}[\sqrt{2+\alpha}\mp\sqrt{2+\alpha'}+(\beta\mp\beta')\mathcal{L}^2]\ , \quad (4.7)$$

with

$$\beta=\frac{\alpha}{48\sqrt{2+\alpha}}[(4+11\alpha)N_{0t}+\alpha(1+2\alpha)]\ ,$$

and $\beta'=\beta(\alpha')$.

Before considering the $O(\mathcal{L}^2)$ expressions for J and χ, it is illustrative to analyze solutions of the lowest-order approximation, in which the $\mathcal{L}^2$ terms are neglected. From (4.4), (4.5), and (4.7) one finds that

$$J=\frac{1}{2\sqrt{2}}\sqrt{1-N_{0t}}N_{0t}(\sqrt{2+\alpha}\pm\sqrt{2+\alpha'})\ , \quad (4.8)$$

$$J_\phi=\tfrac{1}{2}N_{0t}\chi\ . \quad (4.9)$$

Eliminating α by squaring χ of (4.7) and J of (4.8) yields

$$J=\left[\frac{2+r}{2}\right]^{1/2}N_{0t}\left[1-N_{0t}-\frac{\chi^2}{2(2+r)}\right]^{1/2}\ . \quad (4.10)$$

Set $\alpha=r(1+\delta)$ and $\alpha'=r(1-\delta)$, where δ is the fractional shift of the extremum on the transverse branch, relative to the midpoint. The shift δ is, from (4.7) with $\mathcal{L}^2$ neglected,

$$\delta=\frac{\sqrt{2(2+r)}}{r}\frac{\chi}{\sqrt{1-N_{0t}}}\times\left[1-\frac{\chi^2}{2(2+r)(1-N_{0t})}\right]^{1/2}\ . \quad (4.11)$$

In accordance with the discussion of Sec. III, the critical current J_c is defined as that value of J which assumes a maximum for a fixed value of α. Setting $\partial J/\partial N_{0t}|_\alpha=0$ in (4.8) gives $N_{0t}=\frac{2}{3}$. From (4.10) and (4.9) the maximum (critical) transport current J_c and the corresponding J_ϕ are

$$J_c=\tfrac{1}{3}\left[\frac{2}{3}(2+r)\right]^{1/2}\left[1-\frac{3}{2}\frac{\chi^2}{2(2+r)}\right]^{1/2}\ ,$$

and (4.12)

$$J_\phi=\tfrac{1}{3}\chi\ .$$

From (4.11) the shift δ for $N_{0t}=\frac{2}{3}$ is

$$\delta=\frac{\sqrt{6(2+r)}}{r}\chi\left[1-\frac{3}{2}\frac{\chi^2}{(2+r)}\right]^{1/2}\ . \quad (4.13)$$

This equation shows that, for one value of δ there are two distinctly different values of χ. In particular, when $\delta\to 0$ one solution is $\chi\to 0$, corresponding to J_c at its maximum value. The other solution for $\delta\to 0$ is $\chi^2\to(4+2r)/3$, which corresponds to $J_c\to 0$ at ϕ_{c1}. When $J=J_c$, the

branch currents are

$$J_{1,2}=\tfrac{1}{3}\{[\tfrac{2}{3}(2+r)-\chi^2]^{1/2}\pm\chi\}\ . \tag{4.14}$$

For the square ladder $r=1$, and J_c obtained from (4.12) and the corresponding J_1 and J_2 values obtained from (4.14) are shown in Fig. 8. Surprisingly, the qualitative behavior of these asymptotically small $\mathcal{L}$ solutions manifests all essential features of the exact solutions for $\mathcal{L}=\pi/2$, shown in Fig. 7. When $\chi=0$, the value of J_c assumes its maximum of $\sqrt{2}/3$. When $\chi_{c1}=\sqrt{2}$, the critical current $J_c=0$. This happens distinctly away from the second-order phase-transition boundary which occurs at $\chi_{c2}=\sqrt{6}$. The current J_2 changes direction at $\chi=1$, while J_1 assumes its maximum value, $J_{1\max}=\frac{2}{3}$. Furthermore, when $J_c=J_\phi=\frac{1}{3}$, the value of $\delta=3$, a maximum.

In the absence of an injected current, it follows from (4.10) that $N_{0t}=1-\chi^2/(4+2r)$; thus, from (4.9) the shielding current for $J=0$ is

$$J_\phi=\tfrac{1}{2}\chi[1-\chi^2/(4+2r)]\ . \tag{4.15}$$

The current J_ϕ is shown by the dashed curve in Fig. 8 for $r=1$. At $\chi=\sqrt{2}$, J_ϕ reaches its maximum value of $\sqrt{2}/3$, and, at the second-order phase-transition boundary located at $\chi=\sqrt{6}$, both N_{0t} and J_ϕ are zero.

The following physical examination of the critical current phase boundary is based on energy considerations. Neglecting $O(\mathcal{L}^2)$ terms, consistent with the plots in Fig. 8, it follows from (4.3) that the pair density $N(x)=N_{0t}$ on all branches. Thus, the kinetic and condensation energies per branch are from (2.5) and (2.9) $E\mathcal{L}$ and $F\mathcal{L}$, respectively, for the square ladder ($r=1$). The Gibb's free energy G per ladder cell, divided by $\mathcal{L}$, is equal to $E_{01}+E_{02}+3F$. Explicitly,

$$G(J)=\frac{(J+J_\phi)^2}{N_{0t}}+\frac{(J-J_\phi)^2}{N_{0t}}-3N_{0t}(1-\tfrac{1}{2}N_{0t})\ .$$

The energy reference is the normal state $G=0$. For $J=J_c$, using (4.12) and $N_{0t}(J_c)=\frac{2}{3}$, one obtains

$$G(J_c)=-\tfrac{2}{3}\quad\text{for } \chi\le\sqrt{2}\ . \tag{4.16a}$$

For $J=0$, it follows from (4.15), with $N_{0t}=1-\chi^2/6$, that

$$G(0)=-\tfrac{3}{2}(1-\chi^2/6)^2\quad\text{for } \chi\le\sqrt{6}\ . \tag{4.16b}$$

The difference $\Delta G=G(0)-G(J_c)$ is

$$\Delta G=-(2-\chi^2)(10-\chi^2)/24\quad\text{for } \chi\le\sqrt{2}\ .$$

Since $\Delta G\le 0$, the system accommodates the additional kinetic energy due to the supercurrent J_c for $\chi<\sqrt{2}$. For $\chi>\sqrt{2}$ it is evident from (4.12), with $r=1$, that J_c is imaginary, and thus nonphysical. It follows from (4.16a) and (4.16b) that $\partial G/\partial\chi$ is discontinuous at $\Delta G=0$; hence, the phase transition is first order. It should be noted from (2.10) that $G(J)=-3N_{0t}^2(J)/2$, which immediately yields (4.16a) and (4.16b). However, we think that the above analysis is more didactic.

A calculation of the $O(\mathcal{L}^2)$ critical current is found in

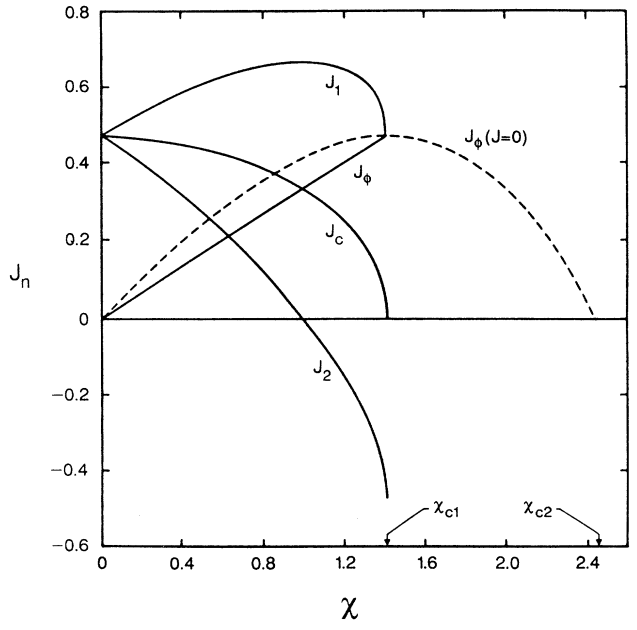

FIG. 8. Shown is the "universal" behavior of the currents J_n as a function of $\chi=2\pi(\phi/\phi_0)\xi(T)/\mathcal{L}$ for $\mathcal{L}\ll\xi$. The dashed curve is the shielding current in the absence of an injected current. The curves are Eqs. (4.12), (4.14), and (4.15) with $r=1$.

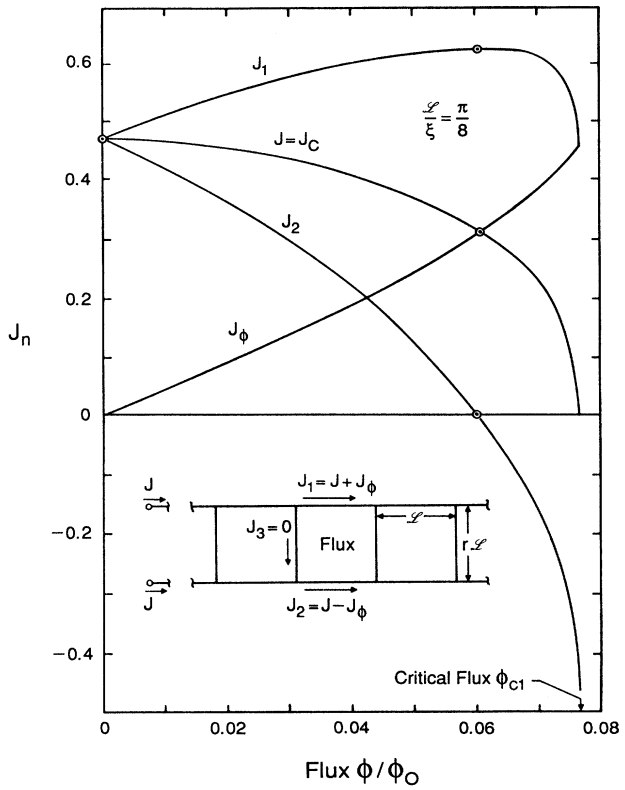

FIG. 9. The currents J_n are shown for $\mathcal{L}/\xi(T)=\pi/8$. Circled points are exact solutions. Solid lines represent the approximate hyperbolic solutions from (4.1) and (4.2).

the Appendix. The various currents are plotted in Fig. 9 as a function of the flux ϕ/ϕ_0 for $\mathcal{L}/\xi=\pi/8$. The solid lines are calculated numerically using the hyperbolic approximation (4.1) and (4.2). The circles points at $\phi=0$ and $\phi/\phi_0=0.0603$ are exact solutions using Jacobian elliptic functions. For $J_c=0$ the exact critical flux is $\phi_{c1}/\phi_0=0.076\,70$. This value is well approximated by the $O(\mathcal{L}^2)$ result (A4) which gives $\phi_{c1}/\phi_0=0.075\,04$. The $O(\mathcal{L}^2)$ approximation of J_c, (A2) and (A3), agrees to within plotting accuracy with the solid lines in Fig. 9, except near the point where $J_\phi=J_c$, due to a singularity in δ (see the Appendix), and at ϕ_{c1} where the error is about 2%.

When only a shielding current $J_\phi=J_1=-J_2$ is present, the shift $\delta=0$. Analytic details for a rectangular ladder are given in the Appendix. For the square ladder, the shielding current as an explicit function of χ is

$$J_\phi(J=0)=\frac{\chi}{2}\left[1-\frac{\chi^2}{6}-\frac{1}{72}\chi^2\left[1-\frac{\chi^2}{4}\right]\mathcal{L}^2\right]. \tag{4.17}$$

Figure 10 shows Eq. (4.17) for $\mathcal{L}/\xi=\pi/8$. This curve corresponds to, within plotting accuracy, the exact numerical solution using elliptic functions. The curve for $J_\phi(J=J_c)$ is taken from Fig. 9. We have checked the accuracy of (4.17) for $\mathcal{L}/\xi=\pi/2$. We find small deviations from the exact solution only to the right of the maximum of J_ϕ. The $O(\mathcal{L}^2)$ approximation is more accurate for $J=0$ than for $J=J_c$ because the distance of the extremum of $N_t(x)$ from a node is always $0.5\mathcal{L}$ for $J=0$. When $J\neq 0$ the distance of the extremum of the extrapolated $N_t(x)$ function from node A can assume a maximum value of $2\mathcal{L}$ when $J_c=J_\phi$. Hence, the latter case requires a higher order approximation.

Figure 11 shows a plot of $\mathcal{L}/\xi(T)$ as a function of ϕ_{c1}/ϕ_0. This is the flux boundary at which the critical transport current of the uniform current mode of the ladder is zero. The solid line for ϕ_{c1}/ϕ_0 is calculated from the approximate hyperbolic equations (4.1) and (4.2). The circles represent exact solutions for $\mathcal{L}/\xi=\pi/8$ and $\pi/2$. Also shown is the second-order phase-transition boundary, denoted by ϕ_{c2}, which is the demarcation between the superconducting and normal states. In the region denoted by S-2, for $\mathcal{L}/\xi<0.55$, only shielding currents exist, linked to the magnetic flux. An imposed transport current will destroy the shielding currents there. Only in region S-1 can a finite transport current be injected without destroying superconductivity.

We now apply the "quasilinear" theory, valid near the second-order phase-transition boundary to the uniform current mode of the square ladder. The phase-transition boundary of the square ladder has been determined in Ref. 3, using the complex order parameter ψ. The approach developed here is based on the quasilinear equations (2.18) and (2.19) which yield the phase transition boundary and an explicit expression for the superfluid ve-

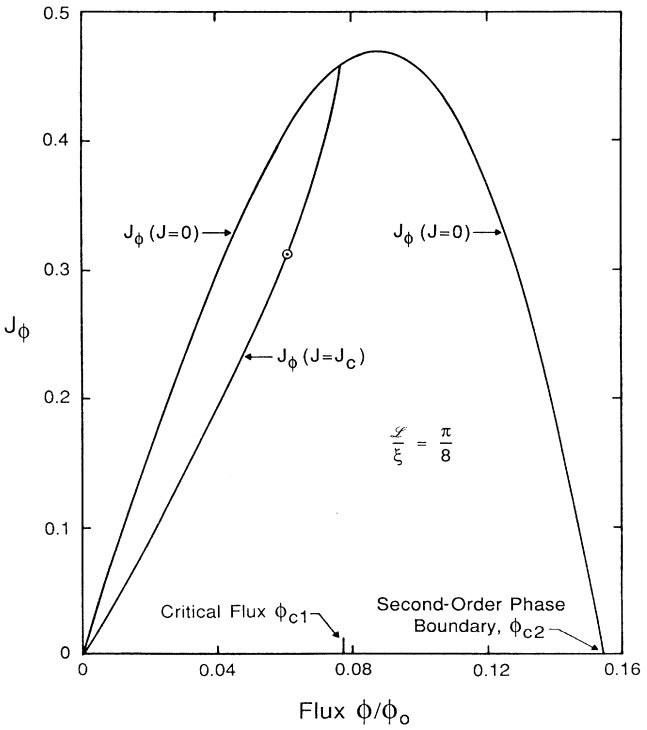

FIG. 10. Shielding current J_ϕ as a function of flux for two values of the transport current J. The upper curve is analytic expression (4.17) for $J=0$, and the lower curve, for $J=J_c$, is taken from Fig. 9. $\mathcal{L}/\xi(T)=\pi/8$.

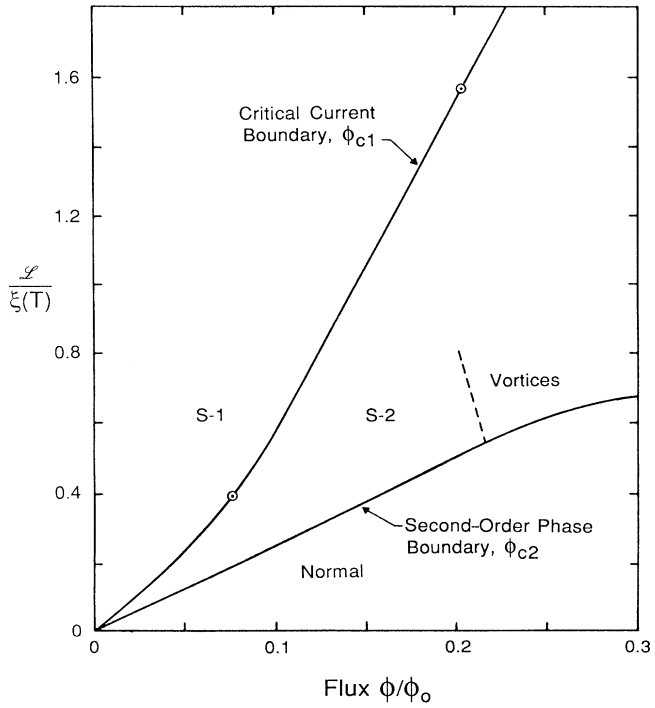

FIG. 11. Temperature-magnetic flux boundary of ladder in the limit of zero lossless transport current, $\mathcal{L}/\xi(T)$ vs ϕ_{c1}/ϕ_0. The second-order phase-transition boundary is denoted by ϕ_{c2}. In region S-2 only shielding currents exist, while in region S-1, both transport and shielding currents are present.

locity Q. The latter is the only nonzero, meaningful transport parameter at the phase-transition boundary.

Applying the first and third equations of (2.18) to a node, noting that for the transverse branch $Q_{0t}=0$, gives the maximum superfluid velocity

$$Q_{01}^2=\frac{3(1+\cos\mathcal{L})}{1+3\cos\mathcal{L}} . \tag{4.18}$$

The flux quantization condition (2.19) is

$$Q_{01}\tan(\mathcal{L}/2)=\tan(\Gamma/4) . \tag{4.19}$$

The second-order phase-transition boundary is obtained by eliminating Q_{01} from (4.18), using (4.19), which yields

$$\sqrt{3/2}\sin(\mathcal{L}/2)=\sin(\Gamma/4) . \tag{4.20}$$

This agrees with the $q=0$ mode derived in Ref. 3, valid for $\phi/\phi_0\lesssim 0.215$. We have thus obtained an explicit expression (4.18) for the maximum superfluid velocity at the phase-transition boundary. It is clear that Q_{01} is nonzero, whereas J_ϕ and $N(x)$ for all x approach zero.

V. CONCLUSION

We have reformulated one-dimensional nonlinear GL equations in terms of real-state variables: superconducting pair density N, kinetic-energy density E, and the imaginary part I of the momentum density $\mathcal{P}$. These state variables are useful tools. They serve as a basis for numerical computation and analytic approximation, and they aid in the physical interpretation of results. Integration of the state-variable equations yields exact algebraic relationships among N, E, and I. Explicitly, E is a quadratic function of N, and I^2 is a cubic function of N. The current density is given by $J^2=NE-I^2$. We have proven two fundamental properties of micronets: (1) The difference between the kinetic-energy density E and the condensation energy density F is always constant along any network branch. (2) The pair density N and the kinetic-energy density E assume opposite extrema at spatial points where the order parameter is an eigenfunction of the momentum operator. The quasilinear state variable theory is not only a different approach for determining the second-order phase-transition boundary, but it also yields the superfluid velocity as the only relevant nonzero transport parameter at the phase boundary.

Approximate solutions for N were found which simplify the numerical procedure considerably. The hyperbolic-function approximation is quite accurate for $\mathcal{L}/\xi$ at least as large as $\pi/2$. Although the solution, using the hyperbolic functions, requires numerical analysis, the procedure is much simpler than that mandated by the exact Jacobian elliptic function solution. This approximation is expected to be quite useful for future micronet analysis.

The theory has been applied to an infinite-ladder micronet. For the uniform shielding current mode, which exists for small magnetic-flux values, we have calculated the maximum supercurrent, as a function of flux, which can be injected from an external source. It is found that external and shielding currents are of the same order of magnitude, so that it is possible to reverse the current direction in one of the wires at some value of the magnetic flux. The critical-current approaches zero at $\phi_{c1}/\phi_0\approx 0.202$ for $\mathcal{L}/\xi(T)=\pi/2$, for example, while the shielding current remains large. It should be emphasized that the critical current of the ladder does not correspond to a situation in which the current in one of the longitudinal branches reaches a maximum value. The critical current becomes zero at a critical magnetic flux $\phi_{c1}(T)$, which is distinct from the second-order phase-transition flux $\phi_{c2}(T)$. For temperatures deep inside the superconducting region and also for temperatures very close to T_c, the temperature dependence of the ϕ_{c1} phase-transition boundary varies approximately as $(\phi_{c1}/\phi_0)^2 \propto 1-(T/T_c)^2$.

We have solved the ladder problem analytically to order $(\mathcal{L}/\xi)^2$ in the limit that $\mathcal{L}/\xi \ll 1$. In the presence of an injected current, for flux less than that necessary to reverse the current in one branch, the $O((\mathcal{L}/\xi)^2)$ approximation is excellent for $\mathcal{L}/\xi$ at least as large as $\pi/8$. In the absence of an injected current, the $O((\mathcal{L}/\xi)^2)$ solution agrees with the exact solution to plot accuracy for $\mathcal{L}/\xi=\pi/8$, and the deviation is small for $\mathcal{L}/\xi=\pi/2$. For $\mathcal{L}/\xi=\pi/8$, the critical current approaches zero at $\phi_{c1}/\phi_0=0.0767$, which is well below the second-order phase-transition boundary located at $\phi_{c2}/\phi_0=0.154$. For $\phi<\phi_{c1}$, it was shown that the ladder can absorb the additional kinetic energy due to an injected supercurrent, whereas for $\phi>\phi_{c1}$, it cannot. At $\phi=\phi_{c1}$ a first-order phase transition occurs.

Experiments regarding critical transport currents on wire networks have been published recently.[16] Critical-current measurements on the microladder at constant temperature as a function of magnetic flux are in progress,[17] and theory and experiments on critical currents of the microladder in zero magnetic flux, as a function of temperature, are discussed in Ref. 18. Electrons on two-dimensional periodic lattices, penetrated by a magnetic field exhibiting fractional flux phenomena, are being studied via a generalization (nonextremum referencing) of the quasilinear method.[15] This study is helpful in understanding flux shuttling on networks, with or without Josephson junctions,[19] and it relates directly to the lattice Coulomb gas,[20] and to the electronic diamagnetism problem at the band edge.[21]

ACKNOWLEDGMENTS

H.J.F. thanks B. Pannetier (Grenoble) and A. López (Bariloche), and S.B.H. thanks P. Erdös (Lausanne), for discussions and for their hospitality at their respective institutions. Partial support from National Science Foundation (NSF) Grant Nos. ECS-85 05627 and INT-88 03025 is acknowledged.

APPENDIX

Returning to (4.5), we analyze the order $\mathcal{L}^2$ equations. Using (4.5) in (4.6), maximizing J with respect to N_{0t} with α fixed gives

$$N_{0t}=\tfrac{2}{3}+\lambda\mathcal{L}^2 \tag{A1}$$

with

$$\lambda=\frac{4}{27}\frac{\sqrt{2+\alpha}\,p\pm\sqrt{2+\alpha'}\,p'}{\sqrt{2+\alpha}\pm\sqrt{2+\alpha'}}\ .$$

Using (A1) in (4.4), the critical current of the square ladder from (4.5) is

$$J_c(\delta)=\frac{1}{3\sqrt{6}}\left[\sqrt{3+\delta}\pm\sqrt{3-\delta}-\frac{1}{48}\left[\frac{3+2\delta}{\sqrt{3+\delta}}(1+\delta)^2\pm\frac{3-2\delta}{\sqrt{3-\delta}}(1-\delta)^2\right]\mathcal{L}^2\right], \tag{A2}$$

and the corresponding expression for J_ϕ is obtained from (A2) by interchanging the upper and lower signs. Using (A1) in (4.7) leads to

$$\chi=\frac{\sqrt{3+\delta}\mp\sqrt{3-\delta}}{\sqrt{6}}\times\left[1-\frac{1}{72}\left[4+\delta^2\mp\frac{3}{2(9-\delta^2)^{1/2}}(133-17\delta^2)\right]\mathcal{L}^2\right]. \tag{A3}$$

Equations (A2) and (A3) disclose a singularity at $\delta=3$ which corresponds to $\phi/\phi_0=0.0625$ in Fig. 9. This singularity arises unavoidably in taking the root of a truncated series expansion of the currents. It is not present in the asymptotic forms given by (4.9)–(4.12), nor in the exact numeric solution.

The solution corresponding to the upper sign in (A2) and (A3) leads, as $\delta\to0$, to $J_c=\sqrt{2}(1-\mathcal{L}^2/48)/3$ at $\chi=0$. The other solution, as $\delta\to0$, leads to $J_c=0$ at χ_{c1}, which is

$$\chi_{c1}=\sqrt{2}(1-\tfrac{47}{48}\mathcal{L}^2)\ . \tag{A4}$$

In the absence of injected current, the shifts $\delta=0$, and $J_\phi=J_1=-J_2$. It follows from (4.4) and (4.7), using the lower sign and $\alpha=r$, that

$$J_\phi=\left[\frac{2+r}{2}\right]^{1/2}N_{0t}\sqrt{1-N_{0t}}\left[1+\frac{r}{48(2+r)}[3(4r^2+13r+4)N_{0t}-(10r^2+27r+8)]\mathcal{L}^2\right] \tag{A5}$$

and

$$\chi=\sqrt{2(2+r)(1-N_{0t})}\times\left[1+\frac{r}{48(2+r)}[(4+11r)N_{0t}+(1+2r)r]\mathcal{L}^2\right]. \tag{A6}$$

At the second-order phase boundary, $N_{0t}=0$. Thus, $J_\phi=0$ and the flux ϕ_{c2} at the second-order phase-transition boundary is determined by

$$\chi_{c2}=\sqrt{2(2+r)}\left[1+\frac{r^2}{48}\left[\frac{1+2r}{2+r}\right]\mathcal{L}^2\right]. \tag{A7}$$

For $r=1$ and $\phi<0.215\phi_0$, Eq. (A7) agrees to $O(\mathcal{L}^2)$ with the exact phase-transition-boundary expression (4.20).

Solving (A6) for N_{0t}, to $O(\mathcal{L}^2)$, yields

$$N_{0t}=1-\frac{\chi^2}{2(2+r)}+\frac{r}{24}\frac{\chi^2}{(2+r)^2}\left[2+6r+r^2-\frac{1}{4}\left[\frac{4+11r}{2+r}\right]\chi^2\right]\mathcal{L}^2 \tag{A8}$$

and the corresponding circulating current is

$$J_\phi=\frac{\chi}{2}\left[1-\frac{\chi^2}{2(2+r)}-\frac{r^2}{24}\frac{(1+2r)}{(2+r)^2}\chi^2\left[1-\frac{3}{4}\frac{\chi^2}{(2+r)}\right]\mathcal{L}^2\right]. \tag{A9}$$

[1]P.-G. de Gennes, C. R. Acad. Sci., Ser. II **292**, 279 (1981).
[2]H. J. Fink, A. López, and R. Maynard, Phys. Rev. B **26**, 5237 (1982).
[3]J. Simonin, D. Rodrigues, and A. López, Phys. Rev. Lett. **49**, 944 (1982).
[4]S. Alexander, Phys. Rev. B **27**, 151 (1983).
[5]R. Rammal, T. C. Lubensky, and G. Toulouse, Phys. Rev. B **27**, 2820 (1983).
[6]A. Behrooz, M. J. Burns, D. Levine, B. Whitehead, and P. M. Chaikin, Phys. Rev. B **35**, 8396 (1987).
[7]F. Nori, Q. Niu, E. Fradkin, and S.-J. Chang, Phys. Rev. B **36**, 8338 (1987).
[8]H. J. Fink, A. López, and D. Rodrigues, Jpn. J. Appl. Phys. **26**, 1465 (1987).
[9]H. J. Fink, Phys. Rev. **177**, 732 (1969); H. A. Schultens, Z. Phys. **232**, 430 (1970).
[10]H. J. Fink and A. López, J. Phys. Lett. (Paris) **46**, L961 (1985).
[11]H. J. Fink and V. Grünfeld, Phys. Rev. B **31**, 600 (1985).
[12]H. J. Fink, V. Grünfeld, and A. López, Phys. Rev. B **35**, 35 (1987); H. J. Fink, J. Loo, and S. M. Roberts, *ibid.* **37**, 5050

(1988).
[13]Y. Y. Yang, B. Pannetier, and R. Rammal, J. Phys. France **49**, 2045 (1988).
[14]Y. Y. Wang, R. Rammal, and B. Pannetier, J. Low. Temp. Phys. **68**, 301 (1987).
[15]S. B. Haley and H. J. Fink (unpublished).
[16]O. Buisson, M. Giroud, and B. Pannetier, Europhys. Lett. **12**, 727 (1990).
[17]O. Buisson, Ph.D. thesis, Université Joseph Fourier, 1990.
[18]H. J. Fink, O. Buisson, and B. Pannetier, preceding paper, Phys. Rev. B **43**, 10 144 (1991).
[19]S. P. Benz, M. S. Rzchowski, M. Tinkham, and C. J. Lobb, Phys. Rev. Lett. **64**, 693 (1990).
[20]S. Teitel and C. Jayaprakash, Phys. Rev. Lett. **51**, 1999 (1983).
[21]Y. Hasegawa, P. Lederer, T. M. Rice, and P. B. Wiegmann, Phys. Rev. Lett. **63**, 907 (1989).